An implicit turbulence model for low-Mach Roe scheme using truncated Navier–Stokes equations

Chung-Gang Li [a,b,*], Makoto Tsubokura [a,b]

[a] *Department of Computational Science, Graduate School of System Informatics, Kobe University, 1-1 Rokkodai, Nada-ku, Kobe 657-8501, Japan*

[b] *Complex Phenomena Unified Simulation Research Team, RIKEN, Advanced Institute for Computational Science, Kobe, Japan*

Correspondence to: Dr. Chung-Gang Li

Assistant Professor

Computational Fluid Dynamics Laboratory

Department of Computational Science

Graduate School of System Informatics

Kobe University, 1-1 Rokkodai, Nada-ku,

Kobe 657-8501, Japan

+81-78-803-6680

[*] *E-mail address*: cgli@aquamarine.kobe-u.ac.jp

ABSTRACT

The original Roe scheme is well-known to be unsuitable in simulations of turbulence because the dissipation that develops is unsatisfactory. Simulations of turbulent channel flow for Re_τ=180 show that, with the `low-Mach-fix for Roe' (LMRoe) proposed by Rieper [J. Comput. Phys. 230 (2011) 5263–5287], the Roe dissipation term potentially equates the simulation to an implicit large eddy simulation (ILES) at low Mach number. Thus inspired, a new implicit turbulence model for low Mach numbers is proposed that controls the Roe dissipation term appropriately. Referred to as the automatic dissipation adjustment (ADA) model, the method of solution follows procedures developed previously for the truncated Navier–Stokes (TNS) equations and, without tuning of parameters, uses the energy ratio as a criterion to automatically adjust the upwind dissipation. Turbulent channel flow at two different Reynold numbers and the Taylor–Green vortex were performed to validate the ADA model. In simulations of turbulent channel flow for Re_τ=180 at Mach number of 0.05 using the ADA model, the mean velocity and turbulence intensities are in excellent agreement with DNS results. With Re_τ=950 at Mach number of 0.1, the result is also consistent with DNS results, indicating that the ADA model is also reliable at higher Reynolds numbers. In simulations of the Taylor–Green vortex at Re=3000, the kinetic energy is consistent with the power law of decaying turbulence with −1.2 exponents for both LMRoe with and without the ADA model. However, with the ADA model, the dissipation rate can be significantly improved near the dissipation peak region and the peak duration can be also more accurately captured. With a firm basis in TNS theory, applicability at higher Reynolds number, and ease in implementation as no extra terms are needed, the ADA model offers to become a promising tool for turbulence modelling.

Keywords: Roe scheme, ILES, TNS, low-Mach-fix, Taylor–Green vortex

1. **Introduction**

Recently, much attention has been centered on compressible turbulent flows at low Mach numbers, such as encountered in aeroacoustics, combustion, and significant heat transfer. Concerning simulations in these areas, the direct use of compressible solvers, e.g., the Roe scheme [1], is unsuitable because energy dissipation performed within the numerical scheme was originally designed for shock waves. Several related numerical methods have been proposed to solve this issue. The first study by Turkel [2] generalizes the artificial compressibility method originally proposed by Chorin [3]. Applying a preconditioning matrix to both incompressible and compressible systems accelerated convergence. This method extends the applicable range of compressible flow equations to low Mach numbers. Weiss and Smith [4] applied the Roe scheme with a preconditioning matrix to develop solutions of the three-dimensional Navier–Stokes equations for low Mach number flows. Thornber [5] uses the local Mach number to scale appropriately the velocity jump at the cell interface to minimize the excessive numerical dissipation on reconstruction. Despite the slight additional computational expense, the noted advantage of this modification is the absence of a cut-off Mach number, which is generally needed for the preconditioning method. Instead of modifying the reconstruction such as [5], Rieper [6] adopted the local Mach number to rescale directly the velocity jump in the characteristic values in the Roe scheme. This simple fix, called `low-Mach-fix for Roe' (LMRoe), can be applied to all reconstructions such as the monotonic upstream-centered scheme for conservation laws (MUSCL), essentially non-oscillatory (ENO) and weighted ENO (WENO) or discontinuous Galerkin methods. For those adopting the Roe scheme, this fix appeared more general than Thornber's approach [5]. Because of its advantages of generality, easy implementation, and also absence of a cut-off Mach number, LMRoe has been applied to diverse fluid problems such as wind turbine flows [7]. However,

we believe a more detailed investigation of the results from LMRoe on turbulence has not been conducted yet.

Apart from the numerical complexities of simulating compressible flows at low Mach numbers, one other issue is how to simulate turbulent flows accurately and efficiently under these situations. If the Reynolds number is too high and/or the available numerical resolution is not sufficient, DNS is not an appropriate choice. In such cases, one must use either the Reynolds-averaged Navier–Stokes-equation (RANS) methods or large eddy simulations (LES). The latter is always preferred for simulations of time-evolving turbulent flows. Tajallipour et al. [8] proposed a self-adaptive upwind method for LES to reduce the numerical dissipation from the Roe scheme as much as possible. The concept is based on the fact that, if the intensity of a local wiggle is smaller than a preset value, the Roe upwind dissipation term can be ignored with the numerical scheme remaining stable. The Roe scheme then becomes a central difference scheme to reduce the numerical dissipation. The separation over the airfoil NACA0025 at angles of attack of 0° and 5° can be successfully captured with this method. As in [8], Ciardi et al. [9] also use a local wiggle to determine whether the numerical dissipation can be reduced. Instead of fully turning the Roe upwind dissipation term on or off as in [8], a small value is adopted to gradually increase or decrease the amount of dissipation. According to their result for channel flow at Re_τ=395, on a scale between 0 and 1 for the Roe upwind dissipation term, 0.3 is the optimal value. However, this optimal value can only be obtained through trial and error. Kotov et al. [10] modified the flow speed indicator originally developed by Li and Gu [11] for the low-speed Roe scheme to control the numerical dissipation. Based on their modification, the flow speed indicator is determined locally during the calculation, so the amount of numerical dissipation can be provided automatically with less parameter tuning. In summary, all

of these results share the same objective, which is to minimize the numerical dissipation as much as possible to prevent adulterating the sub-grid scale (SGS) model while keeping the numerical scheme stable.

Instead of reducing the numerical dissipation and then calculating the SGS model separately to provide an appropriate dissipation such as in [8–10], another way of handling numerical dissipation is to numerically solve the Navier–Stokes equations on a coarse LES, having the truncation error of the numerical scheme serve as a turbulence model, i.e., an implicit LES (ILES). This approach was originally proposed by Boris et al. [12] and reviewed recently in the monograph edited by Margolin and Rider [13]. The ILES methodology is justified based on the practical observation that truncation errors introduce numerical dissipation and its effect is qualitatively similar to the effects of an explicit SGS model. For instance, one can observe a $k^{-5/3}$-energy dependence in numerical simulations by Porter and Woodward [14] of decaying isotropic turbulence performed using an Euler solver. Such results can be used to support the ILES methodology but there are also contradicting results. Garnier et al. [15] analyzed several different shock-capturing Euler schemes applied to decaying isotropic turbulence and found typical behavior associated with low Reynolds number flows rather than that expected from high Reynolds number LES. He determined that ILES provided substantially more numerical dissipation than expected based on the physics of turbulent cascade. Similar conclusions were reached by Domaradzki and Radhakrishnan [16], who showed that the ILES results for rotating and non-rotating turbulence were sensitive to the time step and the method failed to produce theoretically expected results for certain initial conditions and for rotating turbulence. Actually, ILES shares a common feature with all turbulence models; specifically, all of them attempt to dissipate the unphysical energy, which accumulates in small scales because of numerical under-resolution. However, it should be recognized that

numerical dissipation produced from the ILES always lacks physical meaning.

Therefore, neither reducing the numerical dissipation then using the SGS model to reintroduce dissipation nor taking advantage of pure numerical dissipation as an implicit turbulence model; the former wastes calculation time for the same purpose and the latter lacks physical meaning. The aim of this study is to propose a new implicit turbulence model in the LES framework for LMRoe. The new concept revolves around whether numerical dissipation in ILES can be appropriately controlled so as to conform to actual energy transfer from resolved to unresolved, subgrid scales, so that ILES gives physically realistic results. With this in mind, the Roe upwind dissipation term is used to remove the unphysical energy at small scales while using the energy ratio (ER) [17] as a criterion to automatically and physically adjust the amount of dissipation. Thus, the present turbulence model, called the automatic dissipation adjustment (ADA) model, receives the benefit of ILES, which is that no explicit modeling terms are needed, and also places the numerical dissipation term on a firm physical foundation because ER has its roots in the truncated Navier Stokes (TNS) procedure [18]. For the turbulent channel flow a lower Reynolds number of Re_τ=180, we show that LMRoe can significantly reduce numerical dissipation to ensure that the Roe upwind dissipation term potentially establishes an implicit turbulence model. However, with the ADA model, the Roe upwind dissipation term produces a turbulent intensity that is in excellent agreement with incompressible DNS result [19]. For a higher Reynolds number of Re_τ=950, the results demonstrate that the ADA model is also realistic and reliable for higher Reynolds numbers. Besides wall-bounded flows, in the simulation of the Taylor-Green vortex at Re=3000, the dissipation rate is in reasonable agreement with the DNS result [20], indicating that the ADA model is also applicable to isotropic turbulence.

2. Governing Equations

The governing equations are the original Navier–Stokes equations without any additional terms but numerical dissipation to model the SGS effects; i.e., the simulation is LES with implicit turbulence model. Explicitly, they are

$$\frac{\partial U}{\partial t}+\frac{\partial F_1}{\partial x_1}+\frac{\partial F_2}{\partial x_2}+\frac{\partial F_3}{\partial x_3}=0\,. \tag{1}$$

With ρ as the density of fluid, the quantities included in U and F_i are

$$U=\begin{pmatrix}\rho\\ \rho u_1\\ \rho u_2\\ \rho u_3\\ \rho e\end{pmatrix} \tag{2}$$

and

$$F_i=\begin{pmatrix}\rho u_i\\ \rho u_i u_1+P\delta_{i1}-\mu A_{i1}\\ \rho u_i u_2+P\delta_{i2}-\mu A_{i2}\\ \rho u_i u_3+P\delta_{i3}-\mu A_{i3}\\ (\rho e+P)u_i-\mu A_{ij}u_j-k\dfrac{\partial T}{\partial x_i}\end{pmatrix},\quad \forall i=1,2,3\,, \tag{3}$$

where $A_{ij}=\dfrac{\partial u_i}{\partial x_j}+\dfrac{\partial u_j}{\partial x_i}-\dfrac{2}{3}(\nabla\cdot u)\delta_{ij}$ and P is the pressure given by the ideal gas equation

$$P=\rho RT\,. \tag{4}$$

The dynamic viscosity and thermal conductivity of the fluid are based on Sutherland's law:

$$\mu(T)=\mu_0\left(\frac{T}{T_0}\right)^{\frac{3}{2}}\frac{T_0+110}{T+110}\,, \tag{5}$$

$$k(T) = \frac{\mu(T)\gamma R}{(\gamma - 1)Pr}, \tag{6}$$

where ρ_0=1.18 kg/m^3, $\mu_0 = 1.85 \times 10^{-5}$ N·s/m^2, $T_0 = 298.06$ K, $\gamma = 1.4$, $R = 287$ J/kg, and $Pr = 0.72$.

3. Numerical method

The Roe scheme [1] approximates the convective terms in the governing equation given by Eq.(1). Additionally, for future applications, curvilinear coordinates are derived to strengthen the resolution near the wall. Hence, the new governing equation is

$$\frac{\partial \bar{U}}{\partial t} + \frac{\partial \bar{F}_1}{\partial \xi} + \frac{\partial \bar{F}_2}{\partial \eta} + \frac{\partial \bar{F}_3}{\partial \zeta} = 0, \tag{7}$$

where $\bar{U}$ is the conservative form of $(\rho,\rho u_1,\rho u_2,\rho u_3,\rho e)/J$, in which J is the Jacobian transformation matrix. The term $\partial \bar{U} / \partial t$ is obtained by the first-order forward difference and the terms $\partial \bar{F}_1 / \partial \xi$, $\partial \bar{F}_1 / \partial \eta$, and $\partial \bar{F}_1 / \partial \xi$ are obtained by the central difference. Hence, Eq. (7) can be re-expressed as

$$\frac{\bar{U}^{n+1} + \bar{U}^n}{\Delta t} + \frac{1}{\Delta \xi}(\bar{F}^n_{1(i+1/2,j,k)} - \bar{F}^n_{1(i-1/2,j,k)}) + \frac{1}{\Delta \eta}(\bar{F}^n_{2(i,j+1/2,k)} - \bar{F}^n_{2(i,j-1/2,k)}) + \frac{1}{\Delta \zeta}(\bar{F}^n_{3(i,j,k+1/2)} - \bar{F}^n_{3(i,j,k-1/2)}) = 0 \tag{8}$$

and is solved using the third-order accurate total-variation-diminishing Runge–Kutta time stepping method [21]. Specifically

$$\begin{aligned} \bar{U}^{n+1/3} &= \bar{U}^n + R^n \\ \bar{U}^{n+2/3} &= \frac{3}{4}\bar{U}^n + \frac{1}{4}\bar{U}^{n+1/3} + \frac{1}{4}R^{n+1/3} \\ \bar{U}^{n+1} &= \frac{1}{3}\bar{U}^n + \frac{2}{3}\bar{U}^{n+2/3} + \frac{2}{3}R^{n+2/3} \end{aligned} \tag{9}$$

where $R^n = -(\delta_\xi \bar{F}_1^n + \delta_\eta \bar{F}_2^n + \delta_\zeta \bar{F}_3^n)$ and δ_ξ is the central-difference operator.

In the computation of R^n on the right-hand side of Eq. (9), the terms involving F_i in Eq. (3) that depend on the Cartesian coordinates can be divided into two parts. One is the inviscid term $F_{inviscid}$,

$$F_{inviscid} = \begin{pmatrix} \rho u_i \\ \rho u_i u_1 + P\delta_{i1} \\ \rho u_i u_2 + P\delta_{i2} \\ \rho u_i u_3 + P\delta_{i3} \\ (\rho e + P)u_i \end{pmatrix}. \tag{10}$$

The other is the viscous term $F_{viscous}$,

$$F_{viscous} = -\begin{pmatrix} 0 \\ \mu A_{i1} \\ \mu A_{i2} \\ \mu A_{i3} \\ \mu A_{ij} u_j + \lambda \dfrac{\partial T}{\partial x_i} \end{pmatrix}. \tag{11}$$

The LMRoe [6] is employed in the discretization of the $F_{inviscid}$ term and extended to the available range of low Mach numbers using the expression

$$F_{inviscid,i+1/2} = \frac{1}{2}(F_R + F_L) + F_d, \tag{12}$$

where F_d is a dissipation term and can be expressed as

$$F_d = \varepsilon \times F_{Rd}, \tag{13}$$

with F_{Rd} the Roe upwind dissipation term.

In the original Roe scheme [1] and LMRoe [6] or adopting sufficient resolution as in DNS [22], ε in Eq. (13) is always unity to stabilize the numerical scheme. Alternatively, as in [8–10,23–25], ε varied in value between 0 and 1 to reduce dissipation resulting from the Roe upwind dissipation term F_{Rd}. However, in the present study, in Eq. (13) ε relocated as detailed in the next section.

To calculate Eq. (12) and capture the turbulent structures accurately, the

fifth-order MUSCL scheme proposed by Kim and Kim [26] are adopted. Generally speaking, the limiter function should be used to remove the unphysical oscillation due to higher-order interpolations, especially near a discontinuous region such as a shock wave. However, the limiter function affects the turbulent structures through the extra dissipation. Moreover, the Mach numbers involved in the present study are far from those associated with shock waves. Therefore, here the limiter function is abandoned to mitigate its effects. The fifth-order MUSCL without limiter function is then

$$U_{i+1/2}^{L} = 1/60 \times (2U_{i-2} - 13U_{i-1} + 47U_i + 27U_{i+1} - 3U_{i+2}), \tag{14}$$

$$U_{i-1/2}^{R} = 1/60 \times (-3U_{i-2} + 27U_{i-1} + 47U_i - 13U_{i+1} + 2U_{i+2}). \tag{15}$$

Note that the capability of removing non-physical oscillation by the LMRoe scheme is weaker than that of the original Roe. Besides, a limiter function is also abandoned in the present method. As a result, the reduced Mach number range (less than Mach number 0.3) in the present study which appears to be related to the low dissipation of the LMRoe scheme is necessary.

In addition to the inviscid term, the derivative terms in A_{ij} in the viscous term of Eq. (11) are computed using the second-order central difference.

Regarding computational details, the domain is partitioned only in one direction. The message-passing interface (MPI) of the system libraries is used to communicate the necessary data between left and right neighboring nodes. The simulation is performed on a 2.0-GHz 8-core SPARC64 VIIIfx processor.

4. Automatic dissipation adjustment model

4.1 The motivation of ADA model

In the original Roe scheme and LMRoe for DNS, ε in Eq. (13) is always set to unity. When using the original Roe scheme without sufficient resolution to capture all

scales of turbulence, the numerical scheme is strongly dissipative.

A fully developed compressible turbulence in a channel flow is first conducted to investigate the dissipation effects. For its computational domain (Fig. 1), x_1, x_2, and x_3, are in the streamwise, vertical and spanwise directions, respectively, with length, height, and width of l_1, l_2, and l_3; the corresponding velocities are u_1, u_2, and u_3. Isothermal and no-slip boundary conditions are adopted at the channel walls. In the streamwise and spanwise directions, periodic conditions are adopted.

The pressure gradient is the driving force that maintains the continuous flow in the channel. In this simulation, the driving force is always a constant. The method developed by Klein et al. [27] is used to generate the initial condition.

Comparisons of the mean velocity profile and turbulent intensities (Figs. 2 and 3) between the original Roe and LMRoe at Re_τ=180 with $\varepsilon = 1$ show that the original Roe scheme is strongly dissipative. Table 1 lists the relevant parameter settings. Note that none of the turbulence models works in this situation because such models always provide more dissipation to the flow field. This phenomenon of over-dissipation had also been reported in [8–10,23–25]. To reduce dissipation, all of the simulations tried to minimize ε as much as possible subject to maintaining a stable numerical scheme. However, this modification always incurs problems with a lack of physical basis and weak parameter dependence.

In contrast, the results using LMRoe show better agreement. The mean velocity profile and turbulence intensities are significantly improved. The only difference between the original Roe and LMRoe is the Roe upwind dissipation term. This implies that this term in LMRoe provides much more appropriate dissipation than that in the original Roe. Nonetheless, the results of LMRoe still show an overprediction in the streamwise direction and an underprediction in the spanwise and vertical directions, which are typical responses resulting from too much dissipation. However,

this improvement still indicates that if the Roe upwind dissipation term can be suitably regulated, more accurate results can be obtained and then the model becomes an implicit turbulence model.

4.2 The development of ADA model

Encouraged by these results to design a more general and applicable procedure, the dissipation term F_d in Eq. (13) is first examined and rewritten as suggested by Li and Gu [28] in the following form,

$$F_d = \varepsilon \times F_{Rd} = \varepsilon\{-\frac{1}{2}[|U_{RL}|\begin{bmatrix}\Delta\rho\\ \Delta(\rho u)\\ \Delta(\rho v)\\ \Delta(\rho w)\\ \Delta(\rho E)\end{bmatrix} + \delta U\begin{bmatrix}\rho\\ \rho u\\ \rho v\\ \rho w\\ \rho H\end{bmatrix} + \delta p\begin{bmatrix}0\\ n_x\\ n_y\\ n_z\\ U\end{bmatrix}]\}, \tag{16}$$

where U_{RL} *is the cell interface velocity determined by Roe averaged variables [1]*,

$$\delta U = (c - |u|)\frac{\Delta p}{\rho c^2} + \frac{u}{c} f(M)\Delta u, \tag{17}$$

c the speed of sound,

$$\delta p = \frac{u}{c}\Delta p + (c' - |u|)\rho\Delta u \text{, and } c' = f(M)c \tag{18}$$

Note here that Eq. (16) just rearranges the dissipation term F_d for the original Roe and LMRoe, so ε is still unity in [28]. In the original Roe scheme, $f(M)$ is unity, but in LMRoe, $f(M)$ scales between 0 and 1. When applying the original Roe scheme on the situation of lower Mach numbers, the numerical scheme would be too dissipative [6]. In contrast, applying LMRoe on the same situation, because the function $f(M) = Min[1, (|u| + |v| + |w|)/c]$ proposed by Rieper [6] can be appropriately scaled down to M=10^{-3}, the phenomenon of over-dissipation can be solved.

Rieper [6] has shown that checkerboard modes can be suppressed by LMRoe. A clearer analysis was performed in [28]. In LMRoe, the second term in Eq. (16) is used to suppress checkerboard modes whereas the third term is used to decide problems in non-physical behavior. Both terms are related to numerical stability. In [8–10,23–25], ε varies in value between 0 and 1 to reduce the excessive dissipation provided by F_{Rd}. This modification can simply decrease the dissipation but causes numerical instabilities because the second and third terms are affected and hence give rise to an unphysical oscillation. Hence, only the first term, which is the basic upwind dissipation, can be decreased, whereas the second and third terms remain the same as for LMRoe. Therefore, Eq. (16) is modified to

$$F_d = -\frac{1}{2}\{\varepsilon[|U_{RL}|\begin{bmatrix}\Delta\rho\\ \Delta(\rho u)\\ \Delta(\rho v)\\ \Delta(\rho w)\\ \Delta(\rho E)\end{bmatrix}] + \delta U\begin{bmatrix}\rho\\ \rho u\\ \rho v\\ \rho w\\ \rho H\end{bmatrix} + \delta p\begin{bmatrix}0\\ n_x\\ n_y\\ n_z\\ U\end{bmatrix}\}. \qquad (19)$$

After making sure the numerical instabilities caused by the checkerboard problem and non-physical behavior can be prevented because the second and third terms are remained the same as for LMRoe in Eq. (19), we follow the TNS dynamics to derive a criterion to automatically adjust ε. Numerical simulations performed with the TNS equations are equivalent to a sequence of under-resolved DNS, for which energy accumulates at the smallest resolved scales, and incorrect dynamics develops in the long term. Domaradzki et al. [18] removed this excess energy by filtering the flow field at a prescribed filtering interval. Subsequently, Tantikul and Domaradzki [17] proposed a method referred to as automatic filtering criterion to determine when the filter is activated. Because the effects of a filter and the Roe upwind dissipation term in Eq. (12) are similar according to [15], the Roe dissipation term can be used to dissipate the redundant energy similarly to TNS. If the small scale flow field is too

energetic, ε should be increased to dissipate the energy accumulating at small scales; if flow field is already too dissipative, ε should be decreased to avoid attenuating further fluctuations. Note that in TNS once the filtering criterion is activated, the entire flow field is filtered instead of just filtering the areas which are too energetic. Thus the energy will also attenuate even in areas which are not over dissipated. Alternatively, the Roe upwind dissipation term can be modified selectively and locally, only in areas which are over energetic. In other words, ε is a function of time and space coordinates.

To adjust ε automatically, the energy ratio *ER* obtained by [17] should be calculated at every grid point

$$ER = \frac{I(\Delta)}{I(2\Delta)} = \frac{\sum_{i=1}^{3}(u_i - \overline{u}_i)^2}{\sum_{i=1}^{3}(u_i - \hat{u}_i)^2}, \tag{20}$$

where u_i is the original velocity field in the TNS equations, $\overline{u}_i$ the velocity field filtered with the filter width equal to the mesh size Δ, and $\hat{u}_i$ is the filtered velocity field obtained using a filter width of twice the mesh size, 2Δ. The filter used in Eq. (20) to calculate $\overline{u}_i$ and $\hat{u}_i$ are the secondary filters constructed from the top-hat filter G as a primary filter. According to Loh and Domaradzki [29], the top-hat filter with filter widths equal to mesh sizes Δ and 2Δ can be built using curvilinear coordinates as follows:

$$G(\Delta) * u = \frac{1}{8}\left[\frac{2\Delta^+}{\Delta^+ + \Delta^-}u(x_{n-1}) + 6u(x_n) + \frac{2\Delta^-}{\Delta^+ + \Delta^-}u(x_{n+1})\right], \text{ and} \tag{21}$$

$$G(2\Delta) * u = \frac{1}{2}\left[\frac{\Delta^+}{\Delta^+ + \Delta^-}u(x_{n-1}) + u(x_n) + \frac{\Delta^-}{\Delta^+ + \Delta^-}u(x_{n+1})\right], \tag{22}$$

where x_{n-1}, x_n and x_{n+1} are three neighboring grid points, $\Delta^+ = x_{n+1} - x_n$ and

$\Delta^- = x_n - x_{n-1}$.

The secondary filter can be constructed using the approximate deconvolution Q_N of the primary filter G following [30] and is obtained employing

$$Q_N \approx G^{-1} = \sum_{v=0}^{N} (I - G)^v . \tag{23}$$

The filtered velocity fields for the two secondary filters are obtained from

$$\overline{u}_i = (Q_N G(\Delta)) * u_i \text{, and} \tag{24}$$

$$\hat{u}_i = (Q_N G(2\Delta)) * u_i . \tag{25}$$

Fig. 4 in [17] shows the transfer functions for the different filters described above. $k_c^{\Delta} = \pi / \Delta$ is the nominal cutoff wave number for the physical LES scales. Setting $N = 5$ in Eq. (25), the secondary filter completely retains information on a scale larger than the filter width 2Δ and strongly attenuates the energy in a scale between Δ and 2Δ.

Finally, substituting Eqs. (24) and (25) into Eq. (20), the ratio of removed energy by the secondary filter with different filter widths of the primary filters can be calculated. According to [17], this ratio *ER* obtained from the theoretical dissipation, inertial, and Batchelor energy spectra should be in the range 0.007–0.009. This range has been also validated in [31] and [32] for laminar separation bubble flows. An *ER* larger than 0.009 indicates that the energy at small scales is excessive and should be dissipated by increasing ε. An *ER* smaller than 0.007 implies the flow field is already too dissipative and ε should be made as small as possible. Finally, ε is automatically adjusted using

$$\begin{cases} ER < 0.007\,, & \varepsilon = \max[(\varepsilon - \phi), 0]\,, \\ ER > 0.009\,, & \varepsilon = \min[(\varepsilon + \phi), 1]\,, \end{cases} \tag{26}$$

where ϕ is a small increment or decrement used to adjust ε continuously and gradually. Therefore, a smaller value 0.005 is chosen. The initial value of ε is always set unity, which is the same as original Roe scheme [1]. Because the present study focuses on compressible flows at low Mach numbers, the time step has to be smaller to meet the CFL condition for the numerical stability. In such situations, a large number of time steps is needed to reach the desired physical time. Hence, the expectation is that the result is not sensitive to the initial value of ε because ε will reach a suitable range in the very early stage.

5. Results and discussion

5.1 Turbulent channel flow

The computational parameters adopted in the present study and DNS references are tabulated in Table 2. RE180DNS and RE950DNS are the parameters in [19] for $\mathrm{Re}_\tau = 180$ and [33] for $\mathrm{Re}_\tau = 950$, respectively. The results for which LMRoe is used with the ADA model are compared with those for only-LMRoe as an implicit turbulence model. For RE180 and RE950, ε is set to a constant 1.0. For RE180ADA and RE950ADA, the energy ratio is calculated by adjusting ε automatically. All simulations were run until a statistical steady state was achieved. These are the wall resolved LES, where the density of grid points in the x_2 direction near the walls is increased using the hyperbolic tangent function such that the first point away from the wall is at $\Delta x_{2f}^{+} \approx O(1)$. Values of Δx_{2f}^{+}, the distance between the first grid point and the wall in the wall units, are also given in Table 2.

To validate the ADA model, the first simulations for RE180 and RE180ADA at $\mathrm{Re}_\tau = 180$ are performed. All the statistical quantities presented in the present study are averaged for around two non-dimensional time units ($0.5tu_\tau / l_2$) after reaching the statistical steady state. Fig. 5 demonstrates that the statistical steady state has been reached because the sum of the viscous shear stress, Reynolds stress, and Roe dissipation forms a straight line. To identity the statistical steady states in other cases, the same method as above was used and therefore the results are not presented.

Comparisons of the mean velocity and turbulent intensities (Figs. 6 and 7) indicate a much better agreement between RE180ADA and DNS results. In Fig. 6, the distribution of the mean velocity of RE180ADA is in excellent agreement with the incompressible DNS data of Kim et al. [19]. In Fig. 7, RE180ADA only shows a slight overprediction at the peak in the streamwise direction and an underprediction in the spanwise and vertical directions, which are typical features resulting from over dissipation because resolution is coarser than those of DNS. Overall, the results when compared with LMRoe are much more accurate. Evidently, LMRoe with the ADA appears to indicate that the Roe dissipation term provides appropriate dissipation to replicate the results of the implicit turbulence model without adding any extra explicit turbulence terms such as for the Smagorinsky model.

For RE950 and RE950ADA, a coarser resolution compared with RE180 was adopted to investigate the feasibility of the ADA model at higher Reynolds numbers. As for RE950ADA, the mean velocity profiles (Fig. 8) show that the ADA model can significantly improve the result giving a distribution that is in excellent agreement with DNS result. From the distributions of the turbulence intensities (Fig. 9(a)) in the vertical and spanwise directions, the LMRoe results already show good agreement, and so with the ADA model, only a slight improvement near the peak region can be

observed. However, in the streamwise direction, an obvious over-predication near the peak is completely suppressed by the ADA model and the distribution is consistent with the DNS result shown in Fig. 9(b). The results for RE950ADA indicate that not only for low Reynolds numbers, the ADA model also performs well and yields accurate results for higher Reynolds numbers.

5.2 Taylor-Green vortex at Re=3000

Besides the wall bounded flow, the Taylor-Green vortex at Re=3000 was also analyzed to validate the present method in the isotropic turbulence. The computational domain is a cube with sides of length $2\pi L$. Periodic conditions are applied to the three directions. The initial condition is given by

$$u_1 = U_0 \sin(x_1 / L)\cos(x_2 / L)\cos(x_2 / L), \tag{27}$$

$$u_2 = -U_0 \cos(x_1 / L)\sin(x_2 / L)\cos(x_3 / L), \tag{28}$$

$$u_3 = 0, \tag{29}$$

$$p = p_0 + \frac{\rho_0 U_0^{\,2}}{16}[2 + \cos(2x_3 / L)][\cos(2x_1 / L) + \cos(2x_2 / L)], \tag{30}$$

where $p_0 = \rho_0 R T_0$, U_0 is 34.61 *m/s* to ensure the initial Mach number equals 0.1 and L is set to 0.001354 m to ensure the Reynolds number ($\mathrm{Re} = \rho_0 U_0 L / \mu_0$) equals 3000.

The results for which LMRoe is used with the ADA model are compared with those for only-LMRoe as an implicit turbulence model. For N64 and N128, ε is constant at 1.0 and the grid numbers in each direction are 64 and 128, respectively. For N64ADA and N128ADA, the energy ratio is calculated by adjusting ε automatically.

Fig. 10 shows the temporal evolution of the decaying kinetic energy E_k based on the non-dimensional time [$t_{non}=t/(L/U_0)$] and averaged over the computational domain Ω:

$$E_k = \frac{1}{\rho_0 U_0^2 \Omega} \int_\Omega \frac{\rho u_i u_i}{2} \mathrm{d}\Omega . \tag{31}$$

According to Drikakis et al. [34], the power law with −1.2 exponent, is a characteristic of decaying turbulence and should be observed for a short period immediately after that of the dissipation peak at $t_{non} \sim 9$. All results in the present study show that the decay rates consistent with the −1.2 law between $t_{non} \sim 9$ and 11. This is also evidence that the numerical dissipation provided by the compressible solver has the potential to be an implicit turbulence model. However, the results for both N64 and N64ADA are more dissipative than that of N128 and N128ADA. This phenomena can be more clearly observed in Fig. 11, which shows dissipation rates for four cases and the DNS result in [20] using a spectral method with 256^3 resolution. Both of N64 and N64ADA fail to capture the whole decay process because of coarser resolutions. In contrast, the results of N128 and N128ADA are in excellent agreement with the DNS result before $t_{non} \sim 8$. However, thereafter, only N128ADA is in reasonable agreement with the DNS result and the time of the dissipation peak at $t_{non} \sim 9$ is also well captured. Overall, the result for N128ADA suggests that the ADA model is also applicable for simulations of laminar-turbulent transition in the Taylor-Green vortex.

6. Conclusion

The performance of our new implicit turbulence model: ADA model with LMRoe for LES has been demonstrated at low Mach numbers. In the ADA model, the Roe upwind dissipation term automatically adjusts the amount of the dissipation, as

indicated from the TNS method, without the need to tune parameters to replicate an implicit turbulence model. Simulations of the fully developed, compressible turbulent channel flow at low Mach numbers were performed to evaluate the model in wall bounded flows. The results for LES with Re_τ=180 and 950 are in good agreement with the DNS results, implying that the ADA model works for this range of Reynolds numbers. A simulation of the Taylor-Green vortex at Re=3000 was conducted to validate the model in isotropic turbulence. The result showed that, with adequate resolution, this model can also be applied to simulations of transitions during turbulence decay. With the advantages of easy implementation because no additional terms are needed, the near absence of parameter tuning, a physical basis established from the TNS method, and viability for high Reynolds numbers, LMRoe has the potential to become a useful tool for numerical simulations of low-Mach number turbulent flows.

7. Acknowledgement

Several of the results were obtained using the K computer at the RIKEN Advanced Institute for Computational Science (Proposal No. RA000012).

References

[1] P.L.Roe, Approximate Riemann solvers, parameter vectors, and difference schemes, J. Comput. Phys. 43 (1981) 357–372.

[2] E.Turkel, Preconditioned Methods for Solving the Incompressi and Low Speed Compressible Equations, J. Comput. Phys. 298 (1987) 277–298.

[3] A.J.Chorin, A numerical method for solving incompressible viscous flow problems, J. Comput. Phys. 135 (1967) 12–26.

[4] J.M.Weiss, W.A.Smith, Preconditioning applied to variable and constant density flows, AIAA J. 33 (1995) 2050–2057.

[5] B.Thornber, A.Mosedale, D.Drikakis, D.Youngs, R.J.R.Williams, An improved reconstruction method for compressible flows with low Mach number features, J. Comput. Phys. 227 (2008) 4873–4894.

[6] F.Rieper, A low-Mach number fix for Roe's approximate Riemann solver, J. Comput. Phys. 230 (2011) 5263–5287.

[7] M.Carrión, M.Woodgate, R.Steijl, G.Barakos, Implementation of all-Mach Roe-type schemes in fully implicit CFD solvers–demonstration for wind turbine flows, Int. J. Numer. Methods Fluids. 73 (2013) 693–728.

[8] N.Tajallipour, B.B.Owlam, M.Paraschivoiu, Self-Adaptive Upwinding for Large Eddy Simulation of Turbulent Flows on Unstructured Elements, J. Aircr. 46 (2009) 915–926.

[9] M.Ciardi, P.Sagaut, M.Klein, W.N.Dawes, A dynamic finite volume scheme for large-eddy simulation on unstructured grids, J. Comput. Phys. 210 (2005) 632–655.

[10] D.V.Kotov, H.C.Yee, A.A.Wray, B.Sjögreen, A.G.Kritsuk, Numerical dissipation control in high order shock-capturing schemes for LES of low speed flows, J. Comput. Phys. 307 (2016) 189–202.

[11] X.Li, C.Gu, An All-Speed Roe-type scheme and its asymptotic analysis of low Mach number behaviour, J. Comput. Phys. 227 (2008) 5144–5159.

[12] J.P.Boris, F.F.Grinstein, E.S.Oran, R.L.Kolbe, New insights into large eddy simulation, Fluid Dyn. Res. 10 (1992) 199–228.

[13] F.F.Grinstein, L.G.Margolin, W.J.Rider, Implicit Large Eddy Simulation: Computing Turbulent Fluid Dynamics, AIAA J. 46 (2008) 3168–3170.

[14] D.Porter, P.R.Woodward, High-Resolution Simulations of Compressible Convection using the Piecewise-Parabolic Method, Astrophys. J. Suppl. Ser. 93 (1994) 309–349.

[15] E.Garnier, M.Mossi, P.Sagaut, P.Comte, M.Deville, On the Use of Shock-Capturing Schemes for Large-Eddy Simulation, J. Comput. Phys. 153 (1999) 273–311.

[16] J.A.Domaradzki, S.Radhakrishnan, Effective eddy viscosities in implicit modeling of decaying high Reynolds number turbulence with and without rotation, Fluid Dyn. Res. 36 (2005) 385–406.

[17] T.Tantikul, J.A.Domaradzki, Large eddy simulations using truncated Navier–Stokes equations with the automatic filtering criterion, J. Turbul. 11 (2010) 1–24.

[18] J.A.Domaradzki, K.C.Loh, P.P.Yee, Large eddy simulations using the subgrid-scale estimation model and truncated Navier-stokes dynamics, Theor. Comput. Fluid Dyn. 15 (2002) 421–450.

[19] J.Kim, P.Moin, R.Moser, Turbulence statistics in fully developed channel flow at low Reynolds number, J. Fluid Mech. 177 (1987) 133–166.

[20] M.E.Brachet, D.I.Meiron, S.A.Orszag, B.G.Nickel, R.H.Morf, U.Frisch, Small-scale structure of the Taylor-Green vortex, J. Fluid Mech. 130 (1983) 411–452.

[21] C.Shu, S.Osher, Efficient implementation of essentially non-oscillatory shock-capturing schemes, J. Comput. Phys. 77 (1988) 439–471.

[22] C.G.Li, M.Tsubokura, K.Onishi, Feasibility investigation of compressible direct numerical simulation with a preconditioning method at extremely low Mach numbers, Int. J. Comut. Fluid Dyn. 28 (2014) 411–419.

[23] T.T.Bui, A parallel , Finite-volume algorithm for large-eddy simulation of turbulent flows, Comput. Fluids. 29 (2000) 877–915.

[24] W.S.Fu, C.G.Li, W.F.Lin, Y.H.Chen, Roe scheme with preconditioning method for large eddy simulation of compressible turbulent channel flow, Int. J. Numer. Methods Fluids. 61 (2009) 888–910.

[25] W.S.Fu, C.G.Li, M.Tsubokura, Y.Huang, J.A.Domaradzki, An Investigation of Compressible Turbulent Forced Convection by an Implicit Turbulence Model for Large Eddy Simulation, Numer. Heat Transf. Part A Appl. 64 (2013) 858–878.

[26] K.H.Kim, C.Kim, Accurate , efficient and monotonic numerical methods for multi-dimensional compressible flows Part II : Multi-dimensional limiting process, J. Comput. Phys. 208 (2005) 570–615.

[27] M.Klein, A.Sadiki, J.Janicka, A digital filter based generation of inflow data for spatially developing direct numerical or large eddy simulations, J. Comput. Phys. 186 (2003) 652–665.

[28] X.Li, C.Gu, Mechanism of Roe-type schemes for all-speed flows and its application, Comput. Fluids. 86 (2013) 56–70.

[29] K.Loh, J.A.Domaradzki, The subgrid-scale estimation model on nonuniform grids The subgrid-scale estimation model on nonuniform grids, Phys. Fluids.

(1999) 3786–3792.

[30] S.Stolz, N.A.Adams, L.Kleiser, An approximate deconvolution model for large-eddy simulation with application to incompressible wall-bounded flows, Phys. Fluids. 13 (2001) 997–1015.

[31] F.Cadieux, J.A.Domaradzki, Performance of subgrid-scale models in coarse large eddy simulations of a laminar separation bubble, Phys. Fluids. 27 (2015).

[32] F.Cadieux, J.A.Domaradzki, Periodic Filtering as a subgrid-scale model for LES of laminar separation bubble flows, J. Turbul. 17 (2016) 954–965.

[33] J.C.DelAlamo, J.Jiménez, P.Zandonade, R.D.Moser, Scaling of the energy spectra of turbulent channels, J. Fluid Mech. 500 (2004) 135–144.

[34] D.Drikakis, C.Fureby, F.F.Grinstein, D.Youngs, Simulation of transition and turbulence decay in the Taylor-Green vortex, J. Turbul. (2007) 37–41.

Table Captions

Table 1 Settings for the computational parameters for the original Roe and LMRoe with Re_τ=180

Table 2 Setting for the computational parameters of RE180, RE180ADA, RE950, RE950ADA

Table 1. Settings for the computational parameters for the original Roe and LMRoe with Re_τ=180

Mean Mach number	0.051
Mean velocity $< u_1 >$	17.5 m/s
Mean friction velocity u_τ	1.13 m/s
$N_1 \times N_2 \times N_3$	$96 \times 128 \times 72$
Domain size ($l_1 \times l_2 \times l_3$)	$0.0314 \times 0.005 \times 0.0157$ m^3
Nondimensional domain size	$4\pi \times 2 \times 2\pi$
$\Delta x_1^+ \times \Delta x_{2s}^+ (\Delta x_{2l}^+) \times \Delta x_3^+$	$23.6 \times 0.4(4.7) \times 15.7$

Δx_{2s}^+ and Δx_{2l}^+ denote the smallest and largest grid size in the x_2 direction.

Table 2. Settings for the computational parameters of RE180DNS, RE180, RE180ADA, RE950DNS, RE950, RE950ADA

	Re_τ	$\Delta x_1^+ \times \Delta x_{2s}{}^+ (\Delta x_{2l}{}^+) \times \Delta x_3^+$	Nondimensional domain size	$N_1 \times N_2 \times N_3$
RE180DNS[19]	180	$12.0 \times 0.05(4.4) \times 7.0$	$4\pi \times 2 \times 2\pi$	$192 \times 128 \times 160$
RE180	180	$23.6 \times 0.4(4.7) \times 15.7$	$4\pi \times 2 \times 2\pi$	$96 \times 128 \times 72$
RE180ADA	180	$23.6 \times 0.4(4.7) \times 15.7$	$4\pi \times 2 \times 2\pi$	$96 \times 128 \times 72$
RE950DNS[33]	950	$7.8 \times 0.03(7.8) \times 3.9$	$1.0\pi \times 2 \times 0.5\pi$	$384 \times 384 \times 384$
RE950	950	$23.3 \times 0.5(15.4) \times 11.7$	$2.5\pi \times 2 \times 0.5\pi$	$320 \times 256 \times 128$
RE950ADA	950	$23.3 \times 0.5(15.4) \times 11.7$	$2.5\pi \times 2 \times 0.5\pi$	$320 \times 256 \times 128$

	ε	Mean velocity	Mean friction velocity u_τ	l_2
RE180	1.0	17.5 m/s	1.13 m/s	0.005 m
RE180ADA	variable	17.5 m/s	1.13 m/s	0.005 m
RE950	1.0	29.4 m/s	1.48 m/s	0.02 m
RE950ADA	variable	29.4 m/s	1.48 m/s	0.02 m

Figure Captions

Fig. 1 Physical model and computational domain

Fig. 2 Comparison between the original Roe and LMRoe of the normalized mean velocity with Re_τ=180.

Fig. 3 Comparisons between the original Roe and LMRoe of normalized turbulence intensities in the streamwise, spanwise and vertical directions for Re_τ=180

Fig. 4 One-dimensional transfer functions for different filters [17]

Fig. 5 Distributions of the normalized viscous shear stress, Reynolds shear stress, Roe dissipation term and the sum of these three terms

Fig. 6 Comparisons between RE180 and RE180ADA of the normalized mean velocity for Re_τ=180

Fig. 7 Comparisons between RE180 and RE180ADA of normalized turbulence intensities in the streamwise, spanwise and vertical directions for Re_τ=180

Fig. 8 Comparisons between RE950 and RE950ADA of the normalized mean velocity for Re_τ=950.

Fig. 9(a) Comparisons between RE950 and RE950ADA of normalized turbulence intensities in the streamwise, spanwise and vertical directions for Re_τ=950

Fig. 9(b) $x_2 / 0.5l_2$ from 0 to 0.1 in Fig. 9 (a)

Fig. 10 Kinetic energy E_k

Fig. 11 Dissipation rate $-dE_k/dt_{non}$

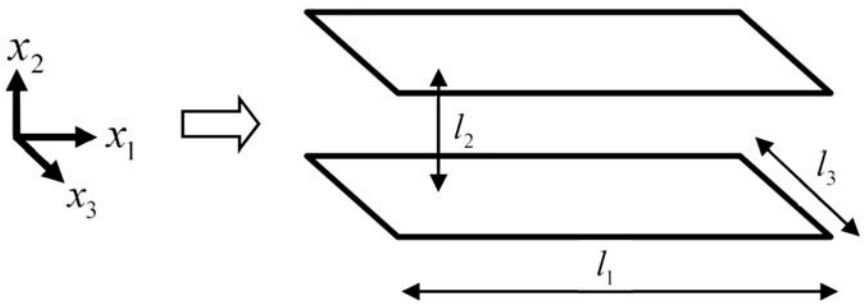

Fig. 1. Physical model and computational domain.

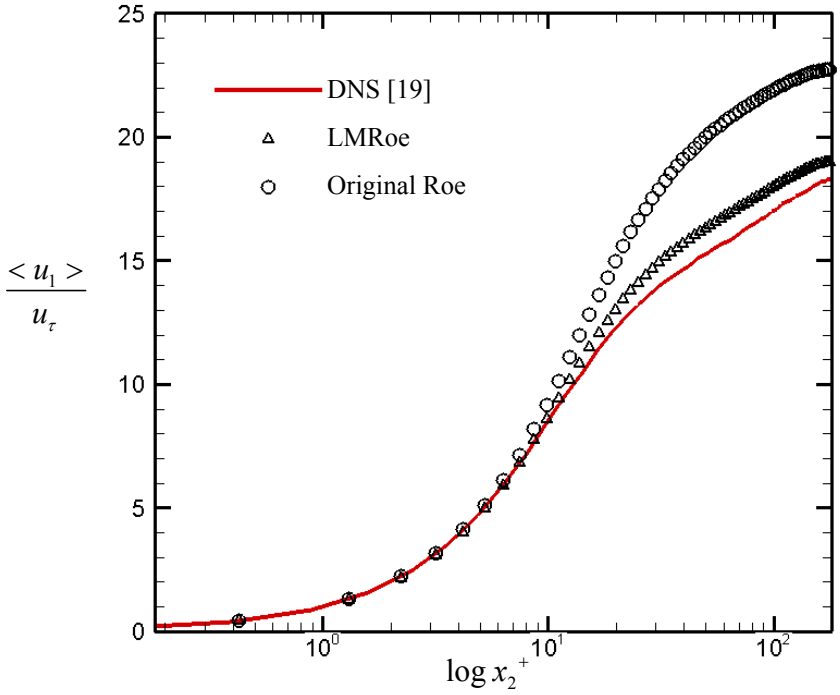

Fig. 2. Comparison between the original Roe and LMRoe of the normalized mean velocity with Re_τ=180.

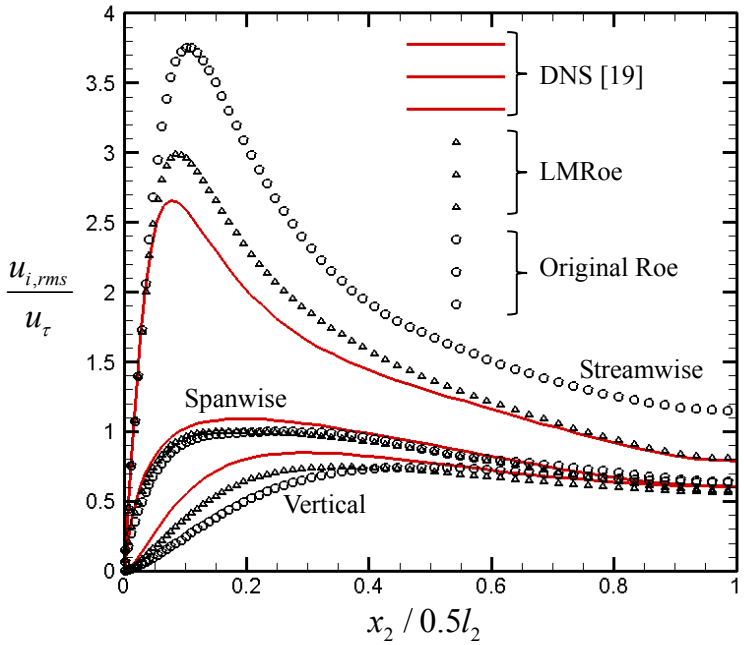

Fig. 3. Comparisons between the original Roe and LMRoe of normalized turbulence intensities in the streamwise, spanwise and vertical directions for Re_τ=180.

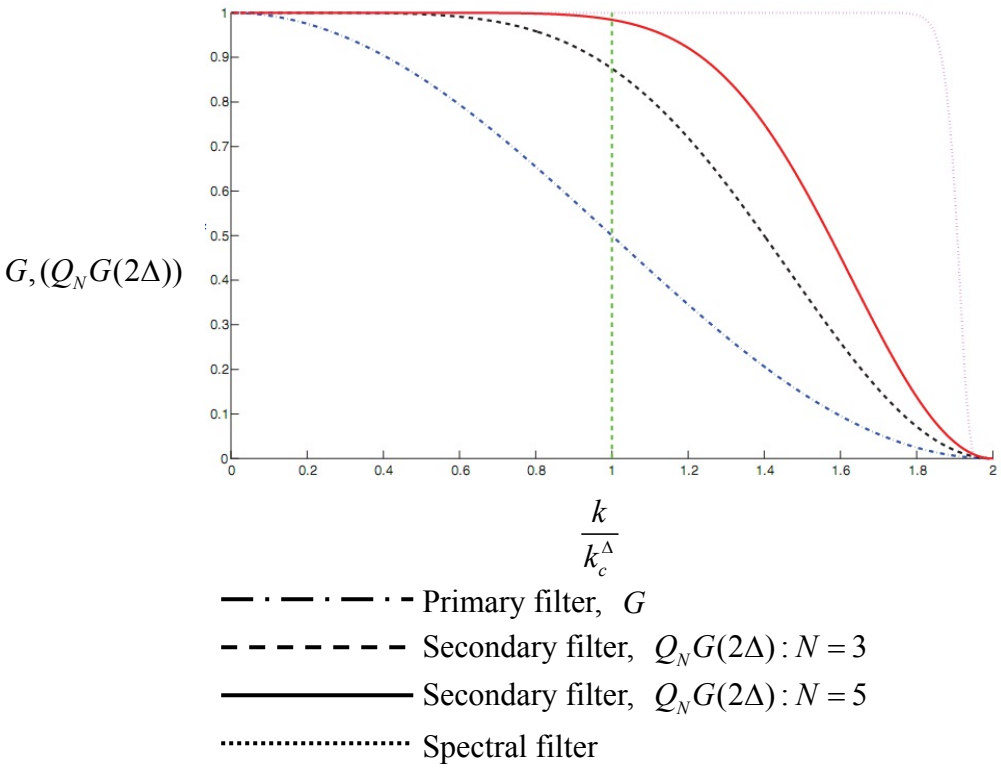

Fig. 4. One-dimensional transfer functions for different filters [17].

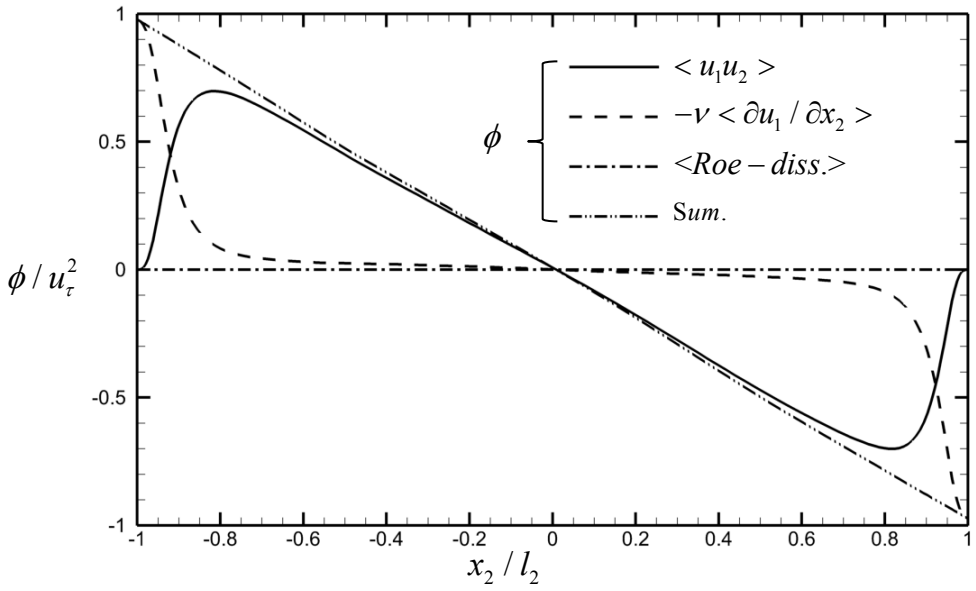

Fig. 5. Distributions of the normalized viscous shear stress, Reynolds shear stress, Roe dissipation term, and the sum of these three terms

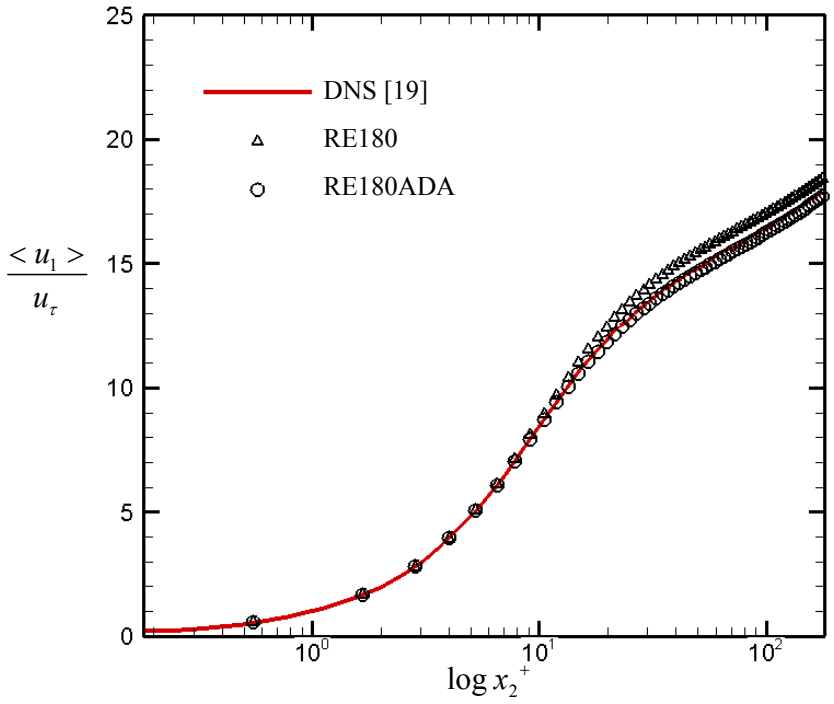

Fig. 6. Comparisons between RE180 and RE180ADA of the normalized mean velocity for Re_τ=180.

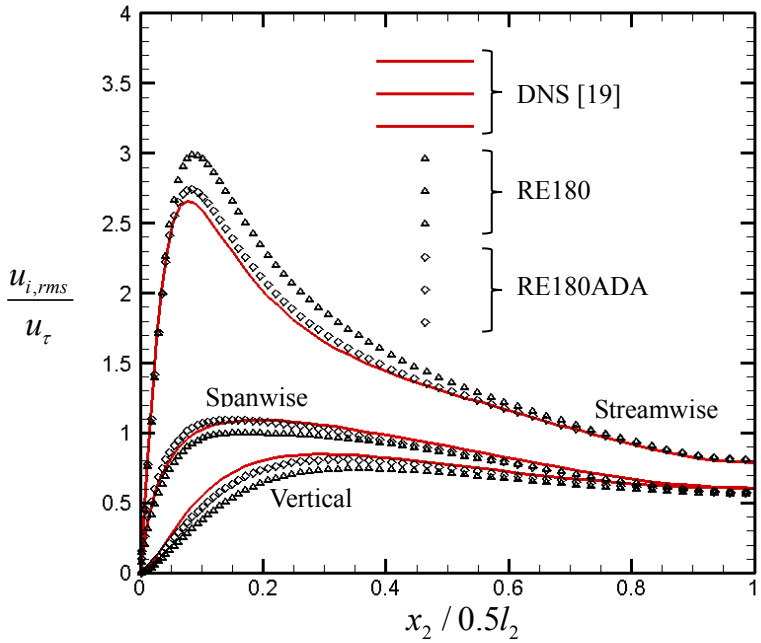

Fig. 7. Comparisons between RE180 and RE180ADA of normalized turbulence intensities in the streamwise, spanwise and vertical directions for Re_τ=180.

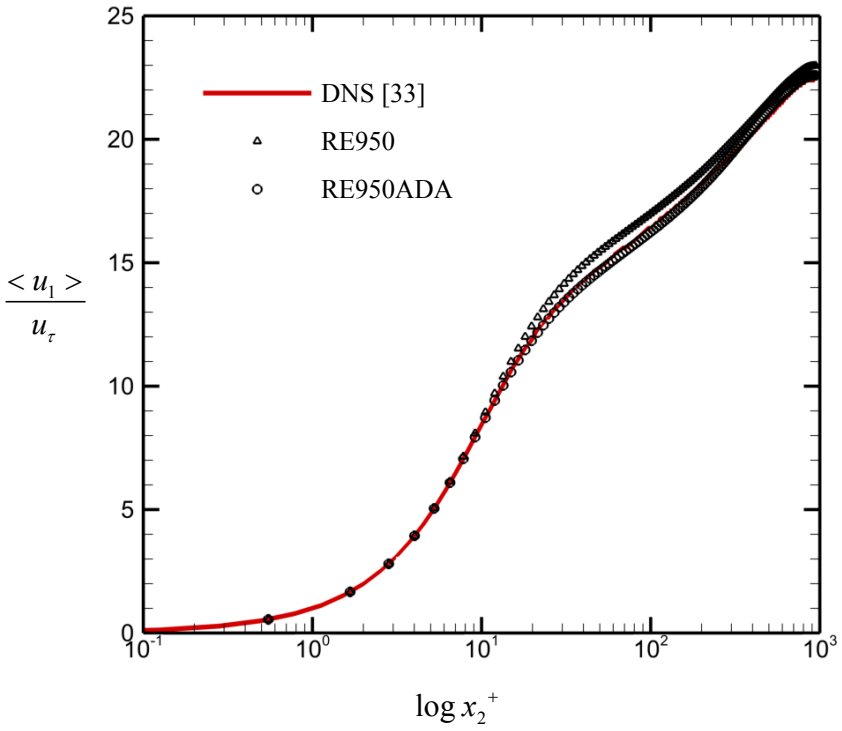

Fig. 8. Comparisons between RE950 and RE950ADA of the normalized mean velocity for Re_τ=950.

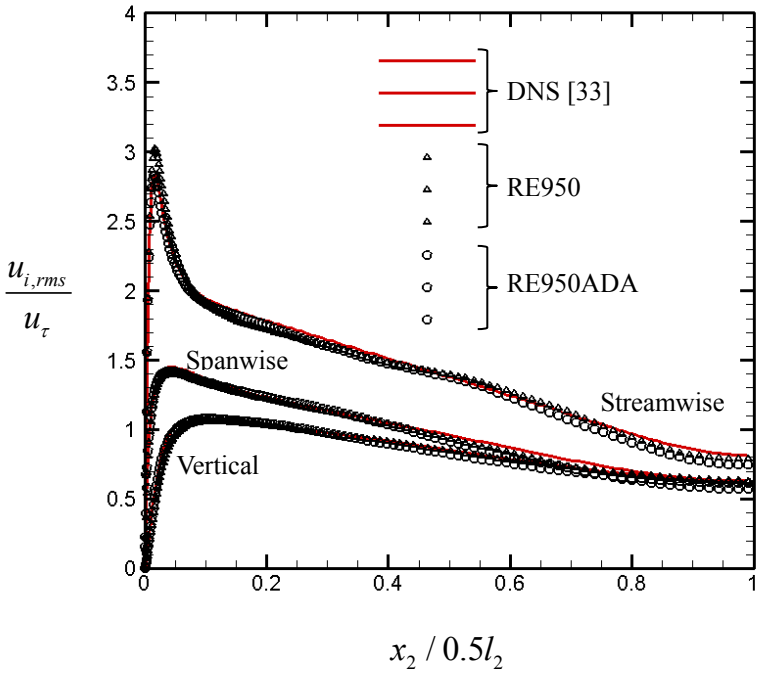

Fig. 9(a). Comparisons between RE950 and RE950ADA of normalized turbulence intensities in the streamwise, spanwise and vertical directions for Re_τ=950.

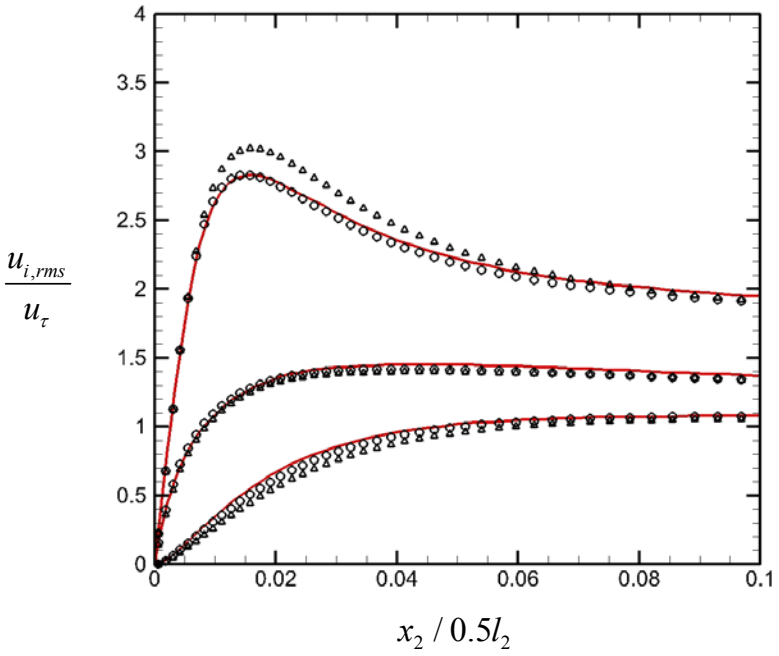

Fig. 9(b). $x_2 / 0.5l_2$ from 0 to 0.1 in Fig. 9 (a)

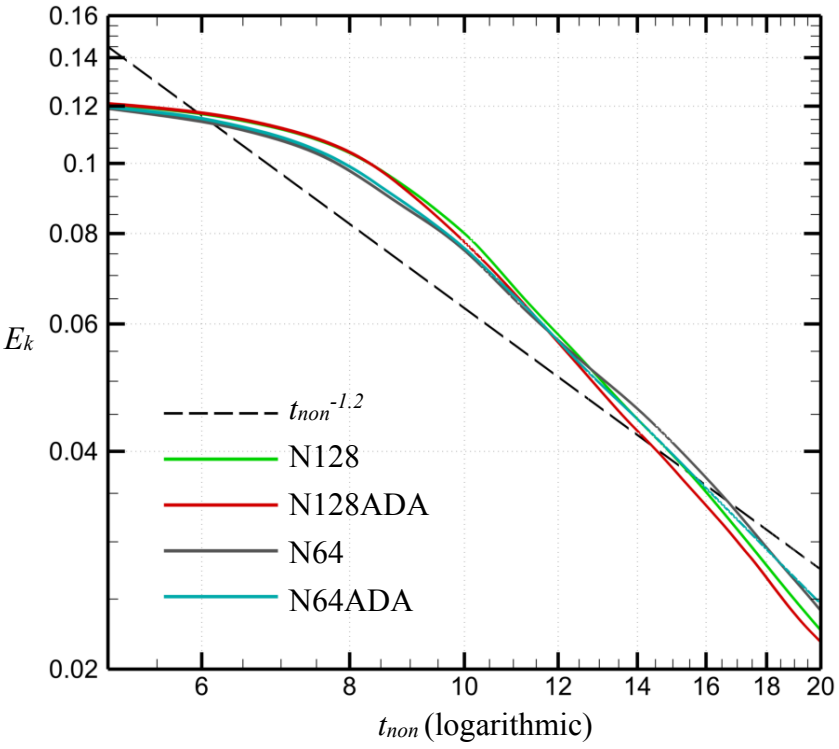

Fig. 10. Kinetic energy E_k

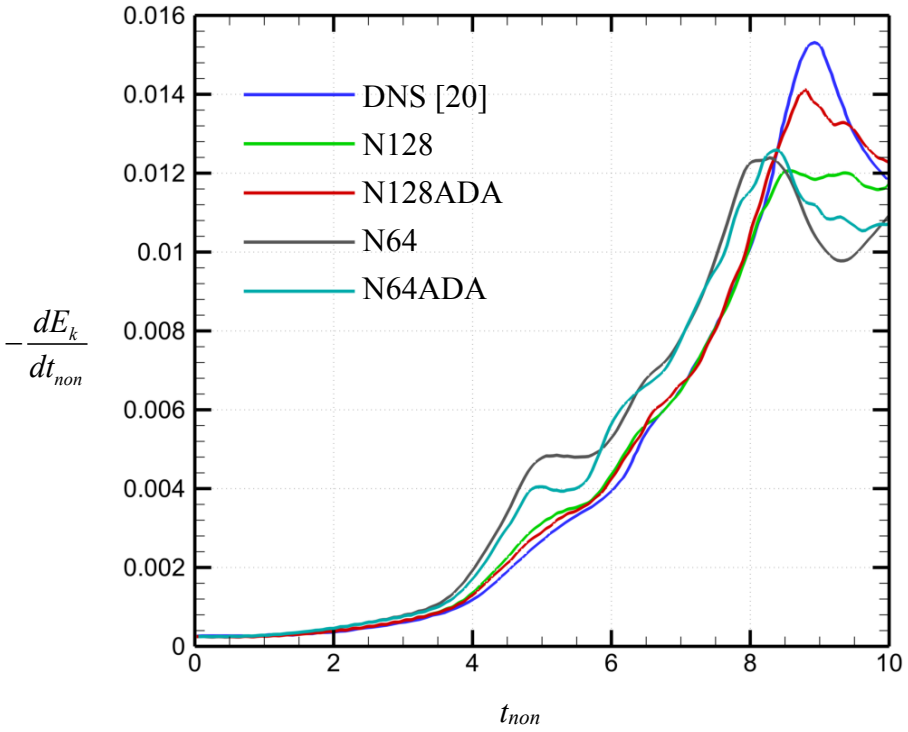

Fig. 11. Dissipation rate $-dE_k/dt_{non}$